



Optomechanical Imaging: Biomechanical and Hemodynamic Responses of the Breast to Controlled Articulation

Rabah Al abdi¹, Gavriel Feuer¹, Harry L. Graber^{1,2}, Subrata Saha¹, and Randall L. Barbour^{1,2}

¹SUNY Downstate Medical Center, 450 Clarkson Ave, Brooklyn NY 11203

²NIRx Medical Technologies LLC, 15 Cherry Lane, Glen Head NY 11545, USA



Abstract:

The optomechanical response of the breast was explored during fine articulation, as a function of the applied force protocol. Comparisons between calculated internal pressure or stress maps and reconstructed hemodynamic images show strong correlations.

Introduction:

There are many instances where the details of blood delivery to tissue and bulk fluid redistribution among the various vasculature compartments can be impacted by disease or trauma. For instance, a common phenotype of breast cancer is derangements in hemodynamic states accompanied by increased tissue stiffness and local edema [1].

Motivated by the hypothesis that externally applied mechanical forces can produce distinct dynamic responses among these compartments, we have recently developed working technology as a new approach for assessment of pathology of the breast and other soft tissues. Principal elements of this technology, referred to as optomechanical imaging [2], include concurrent bilateral measures of the viscoelastic and hemodynamic properties of the breast in response to a wide range of controlled articulation maneuvers. Encouraging evidence was reported of high-contrast tumor detection in response to these maneuvers [2].

To better appreciate the influence that externally applied forces can be expected to have on internal fluid shifts, here we have compared the measured hemodynamic response of the breast to modeled estimates of internal mechanical forces, across a variety of applied articulation maneuvers.

Taking the lead from Darling *et al.* [3], we have estimated the internal thermodynamic pressure p (alternatively referred to as the interstitial fluid pressure), and other related metrics, of the breast in response to specified maneuvers. Results obtained strongly suggest that mechanical modeling is a useful approach to predicting bulk hemodynamic responses to controlled articulations.

Methods:

Simultaneous bilateral breast imaging was performed using a newly developed optomechanical imaging system described by Al abdi *et al.* [2]. The described system provides for high optode-density CW-NIRS DOT imaging, accommodates a wide range of breast sizes, and simultaneously measures the viscoelastic response of the breast to finely controlled articulations. Fig. 1 shows a photograph of the sensing heads used for data collection and articulation. Fig. 2 shows the 16 articulating elements (AEs) and their classification based on their positions in relation to the breast.

Articulations include:

- Quasistatic: full-compression protocols, which involved applying 7.1 N of force to every articulating element (AE); partial compression involved applying similar forces either to the mediolateral AEs only, or to the craniocaudal AEs only.
- Creep compression was implemented by applying force to all AEs and holding this force constant by moving AEs to compensate for any decrease that might result from tissue relaxation.
- Vibratory compression was implemented by applying force by all AEs and then returning to the initial force level in a short time (20 cycles, 15 s/cycle).
- Stepwise compression was implemented by increasing the force applied to all AEs by 0.5 N per step, then waiting only 20 s for tissue relaxation prior to the next step.
- Wave-like compression involves applying force to the different AEs in succession, starting with the lateral AEs and progressing to the medial ones, with an interval of 5 s per AE.

Thermodynamic pressure (p) and effective stress (σ_e) were calculated via a finite element analysis, performed on a homogeneous model of breast tissue that has mechanical properties appropriate for adipose tissue (i.e., Young's modulus = 19 kPa, Poisson's ratio = 0.495 [3]). The geometric model considered, shown in Fig. 3b, contains 3,908 nodes and 16,761 elements, and represents an approximation to the geometry of a typical breast when placed inside the breast imager's sensing head. Mechanical pressure, principal stresses, and principal strains were computed using a nonlinear finite element software called FeBio [4], and p and σ_e were calculated using Eq. (1) and (2).

3D optical image reconstruction was performed using the Normalized Difference Method of Pei *et al.* [5].

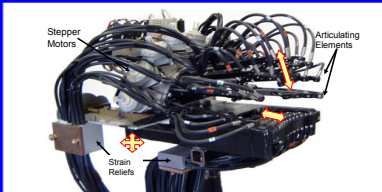


Fig. 1: a photograph of the sensing head.

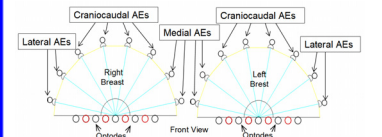


Fig. 2: A schematic of the location of the articulating elements (AEs) relative to the left and right breasts.

$$\sigma_e = \sqrt{(\sigma_1 - \sigma_2)^2 + (\sigma_2 - \sigma_3)^2 + (\sigma_3 - \sigma_1)^2} / 2 \quad (1)$$

$$p = \bar{p} + (\lambda + 3\mu/2) \text{tr}(\mathbf{e}) \quad (2)$$

p : thermodynamic pressure, \bar{p} : mechanical pressure, $\text{tr}(\mathbf{e})$: principal strains, σ_e : effective stress, σ_i are the three principal stresses.

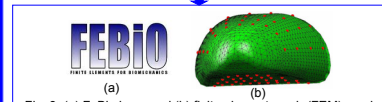


Fig. 3: (a) FeBio logo, and (b) finite element mesh (FEM) used for hemodynamic image-reconstruction computations.

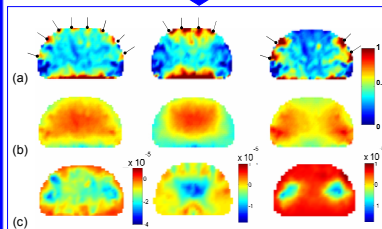


Fig. 4: (a) Calculated thermodynamic pressure, (b) calculated effective stress, and (c) reconstructed AHT for a healthy subject (57 year-old woman with D breast size and BMI of 27).

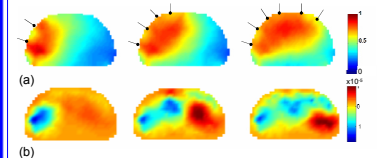


Fig. 5: (a) Calculated effective stress during progressive wave-like compression (from left to right, where black markers indicate the active articulating elements); (b) reconstructed ΔHbT for a healthy subject (43 year-old woman with D breast size and BMI of 35).

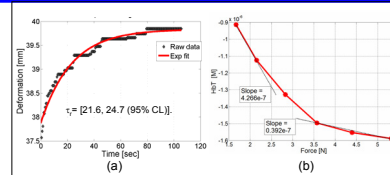


Fig. 6: (a) average creep under 7.1 N constant force, and (b) total hemoglobin concentration vs. applied force, during stress relaxation.

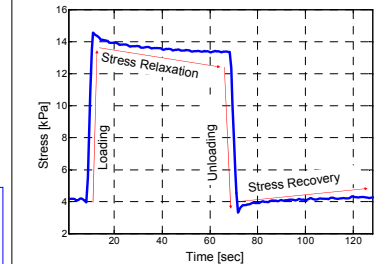


Fig. 7: Stress relaxation and recovery during quasi-static 7.1 N full compression.

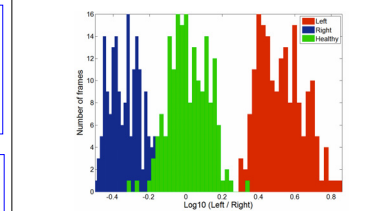


Fig. 8: A histogram of HbDeoxy SSD ratios, during full and mediolateral stress relaxation. Subjects: 56/y/o with 2 cm DCIS in the left breast (red); 36 y/o with 1 cm IDC in the right breast (blue), and 59 y/o healthy subjects (green).

Table 1: patients' clinical information

Group	Number	Age (yrs)	BMI
Cancer	17	55.7 ± 10.5	33.4 ± 8.1
Benign	29	49.9 ± 9.4	32.0 ± 6.1
Healthy	24	54.3 ± 12.1	30.1 ± 4.3

Cancer: 11 invasive ductal carcinoma, 2 invasive mammary carcinoma, 2 ductal carcinoma in situ, and 2 Intraductal carcinoma. Tumor dimensions range from 0.5 cm to 6 cm.

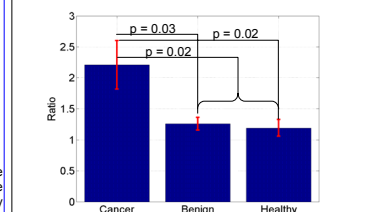


Fig. 9: group mean and standard error of HbDeoxy SSD ratios, during mediolateral force relaxation.

Results:

Axial views of the calculated p and σ_e , following normalization of each image to its maximum value, are shown in Fig. 4a and 4b, respectively. Corresponding changes in the apparent total hemoglobin responses (ΔHbTot) derived from measurements taken on a healthy subject, are shown in Fig. 2c. Inspection of the full-compression pressure maps reveals that p is largest at the breast surfaces and decreases rapidly toward the center, while σ_e tends to increase in moving from the surface to the center. The medial and lateral compression creates local maxima in p and σ_e maps in the medial and lateral regions, while the craniocaudal compression creates local maxima in p and σ_e in the craniocaudal regions and low p and σ_e in the medial and lateral regions. These localized regions of high p and σ_e will produce pressure gradients within the breast tissue, which can produce directed blood flow and tissue displacement from high-pressure to low-pressure regions. Similar pressure and hemodynamic response patterns were noticed in the wave-like compression, which is shown in Fig. 5. Hence the direction of blood flow can be controlled by engaging different subset of AEs with different compression force values.

In the creep compression, tissue relaxation produces a decrease in the applied force, which triggers AEs to compensate for this decrease. Fig. 6a shows the average time-dependent movement of all AEs for a 43 year-old, otherwise healthy subject. As shown, the time-dependent deformation is essentially an exponential function.

The force-dependent hemodynamic response to step-wise compression, for the same subject as in Fig. 6a, is shown in Fig. 6b. Inspection reveals that the rate of change of HbTot is higher at low pressure, and this high rate indicates exclusion of blood from vascular compartments having high apparent vascular compliance (e.g., veins and capillaries). On the other hand, this rate decreases at high compression force, which indicates exclusion of blood from vascular compartments of low apparent vascular compliance (e.g., arteries). This force-dependent hemodynamic response was also reported by Carp *et al.* [6].

An example of the viscoelastic response observed during a quasi-static full compression is shown in Fig. 8. Four phases are identified: loading, stress relaxation, unloading, and stress recovery.

To produce biomarkers sensitive to breast cancer, the spatial variability across the hemodynamic responses of transmission sensor array was calculated (standard deviation) for the left and right breast ($\text{SSD}_L/\text{SSD}_R$). Fig. 8 shows a histogram of the calculated $\text{SSD}_L/\text{SSD}_R$ for two cancer subjects and a healthy control. As shown, the spatial variability in the affected breast is higher than in the contralateral unaffected breast.

Fig. 9 shows the mean and standard error for $\text{SSD}_{\text{Affected breast}}/\text{SSD}_{\text{Unaffected breast}}$ for cancer and benign-pathology subjects, and $\text{SSD}_L/\text{SSD}_R$ for healthy subjects. (See Table 1 for descriptive statistics on subject age and BMI) These ratios were calculated for deoxyhemoglobin (HbDeoxy) during the stress relaxation following mediolateral quasi-static compression. The cancer group mean is significantly higher than those of the other subject groups.

Summary:

Applying pressure to the breast surface creates a complex heterogeneous pressure distribution within the tissue, and the spatial distribution of these forces is a function of the applied articulation maneuver and the tissue's material mechanical properties. The observation that there is a strong correlation between the measured hemodynamic response and computed spatial distributions of mechanical forces suggests that the simple poroelastic model considered [Eqs. (1),(2)] can serve as a useful guide to predicting expected hemodynamic responses. A wide range of differential responses that serve to discriminate healthy from cancerous breasts can be derived from hemodynamic responses during mechanical provocations.

References

- [1] P. Vaupel, "Blood perfusion and microenvironment of human tumors, implications for clinical radiooncology," in *Tumor Blood Flow*, M. Molls and P. Vaupel, eds. (Springer, 2000), 41-45.
- [2] R. Al abdi, H.L. Graber, Y. Xu, and R.L. Barbour, "Optomechanical imaging system for breast cancer detection," *J. Optical Society of America A* 28, 2473-2493 (2011).
- [3] A. L. Darling, P. K. Yalavarthy, M. M. Doyle, H. Delghani, and B. W. Pogue, "Interstitial fluid pressure in soft tissue as a result of an externally applied contact pressure," *Phys. Med. Biol.* 52, 4121-4136 (2007).
- [4] The University of Utah, "FeBio," <http://mri.usc.lutah.edu/software/febio>.
- [5] Y. Pei, H.L. Graber, and R.L. Barbour, "Influence of systematic errors in reference states on image quality and on stability of derived information for DC optical imaging," *Applied Optics* 40, 5755-5769 (2001).
- [6] S. A. Carp, J. Sell, Q. Fang, R. Moore, D. B. Kopans, E. Rafferty, and D. A. Boas, "Dynamic functional and mechanical response of breast tissue to compression," *Optics Express* 16, 16054-16078 (2008).

Acknowledgements

This research was supported by the National Institutes of Health (NIH) grant R41CA096102, the U.S. Army grant DAMD017-03-C-0018, the Susan G. Komen Foundation, the New York State Department of Health (Empire Clinical Research Investigator Program), the New York State Foundation for Science, Technology and Innovation—Technology Transfer Incentive Program (NYSTAR-TIPP) grant C020041, and NIRx Medical Technologies.